Supplementary Information

Observation of large spin-polarized Fermi surface of a magnetically proximitized semiconductor quantum well

Harunori Shiratani[1*], Kosuke Takiguchi[1*], Le Duc Anh[1,2,3], and Masaaki Tanaka[1,4,5]

[1] *Department of Electrical Engineering and Information Systems, The University of Tokyo, Bunkyo-ku, Tokyo 113-8656, Japan*

[2] *Institute of Engineering Innovation, The University of Tokyo, Bunkyo-ku, Tokyo 113-8656, Japan.*

[3] *PRESTO, Japan Science and Technology Agency, Kawaguchi, Saitama, 332-0012, Japan*

[4] *Centre for Spintronics Research Network, The University of Tokyo, Bunkyo-ku, Tokyo 113-8656, Japan.*

[5] *Institute for Nano Quantum Information Electronics, The University of Tokyo, Meguro-ku, Tokyo 153-8505, Japan*

[*]: Equal contribution to this work

Spin splitting estimation by proximity magnetoresistance (PMR) curve fitting

In our previous study of the magnetic proximity effect (MPE) in InAs/(Ga,Fe)Sb bilayer heterostructures[1], the spin splitting energy evaluation is performed by magnetoresistance (MR) curve fitting. Although this estimation is not a direct method unlike the quantum oscillation analysis which is a main scope of this paper, this MR curve fitting can figure out the phenomenological trend of spin splitting energy against the carrier concentration.

The model referred to as the modified Khosla-Fischer model was used in our previous study[1,2], as described below:

$$\frac{\Delta\rho}{\rho} = -a^2 \ln\left(1 + b^2\left(\frac{B}{\mu_0}\right)^2\right) + \frac{c^2\left(\frac{B}{\mu_0}\right)^2}{1 + d^2\left(\frac{B}{\mu_0}\right)^2}, \tag{S1}$$

where

$$a = A_1 J D(\epsilon_\mathrm{F})[S(S+1) + \langle M^2\rangle], \tag{S2}$$

$$b^2 = \left[1 + 4S^2\pi^2\left(\frac{2JD(\epsilon_\mathrm{F})}{g}\right)^4\right]\left(\frac{g\mu_\mathrm{B}}{\alpha k_\mathrm{B}T}\right)^2, \tag{S3}$$

$$c^2 = \frac{\sigma_1\sigma_2(\mu_1+\mu_2)^2}{(\sigma_1+\sigma_2)^2}, \tag{S4}$$

$$d^2 = \frac{(\sigma_1\mu_2 - \sigma_2\mu_1)^2}{(\sigma_1+\sigma_2)^2}. \tag{S5}$$

B is an external magnetic field applied perpendicular to the film plane. In eq. (S2) and (S3), A_1 is a constant representing the contribution of spin scattering to the whole MR, α is a numerical factor that is on the order of unity, $D(\epsilon_\mathrm{F})$ is the density of states at the Fermi level ϵ_F, g is the effective Lande g-factor of the InAs quantum well, $\langle M^2\rangle$ is the averaged squared magnetization, S is the localized spin moment of (Ga,Fe)Sb (we assume $S = 5/2$ for Fe^{3+} ions in (Ga,Fe)Sb), and J is the *s,p-d* exchange interaction energy at the bilayer interface. In eq. (S4) and (S5), σ_i and μ_i represent the conductivity and mobility of electron carriers in InAs, respectively. The subscripts 1 and 2 of each parameter denote the majority and minority spins, respectively. In eq. (S1), the first term, which gives a negative MR component is due to the Kondo scattering of electron carriers in the InAs by the localized Fe spins at the (Ga,Fe)Sb interface. The second term, which gives a positive MR component, is caused by the exchange interaction between the transport carriers in InAs and the localized Fe spins at the InAs/(Ga,Fe)Sb interface.

Using eq. (S5), spin splitting energy $\Delta^{\mathrm{KF}}_{\mathrm{MPE}}$ in the two-dimensional electron system can be obtained by[1,2]

$$\Delta^{\mathrm{KF}}_{\mathrm{MPE}} = 2\pi\hbar^2\frac{n}{\mu m^*}d \tag{S6}$$

where n is the electron carrier density, μ is the electron mobility. m^* is the effective mass of electrons obtained by Fig. S7. n and μ are estimated by the ordinary Hall effect measurement.

The fitting results at each gate voltage (-12 V $< V_\mathrm{g} <$ 5 V) are shown in Fig. S6. For reliable fitting and reasonable estimation of $\Delta^{\mathrm{KF}}_{\mathrm{MPE}}$, we limit the fitting region of B to neglect the effect the oscillatory components in MR curve as; 0 T < B < 5 T in V_g = −12 V, −7 V, 0 V, and 5 V; 0 T < B < 5.4 T in V_g = −5 V and −3 V; 0 T < B < 9 T in V_g = 2 V and 3 V. The obtained $\Delta^{KF}{}_{MPE} - n$ characteristic is shown in Fig. S3. The trend indicates that $\Delta^{KF}{}_{MPE}$ linearly decreases in the lower n region 2.9×10^{12} [cm^{-2}] < n < 4.7×10^{12} [cm^{-2}]. This fact is the main reason for the assumption of $\Delta_{MPE} = \Delta_0 - \xi n$ and eq. (4) in the main manuscript.

Effective mass variation under the strong magnetic proximity effect

We investigate the V_g-dependence of m^*. Evaluating m^* is not only required for the device design, but also essential to scrutinize the electronic states with MPE. Under MPE, s-d hybridization, which is considered to be induced at the InAs/(Fa,Fe)Sb interface, deforms the original Fermi surface of the s-orbital of the InAs conduction band[3]. From eq. (3) in the main manuscript, the temperature dependence of the SdH oscillation magnitude provides the information of the effective mass. Fig. S4 shows SdH oscillations of sample A measured in the wide range of V_g at various temperatures (2 – 20 K). The SdH oscillations in the InAs QW remain even at 20 K reflecting the high coherency of the InAs channel. The FFT spectra are shown in Fig. S5. The temperature dependence of FFT peak intensity is fitted by the the Lifshitz - Kosevich (LK) theory, as shown below[4].

$$\Delta\sigma_{xx} \propto \frac{2\pi^2 k_B T}{\hbar\omega_c} \bigg/ \sinh\left(\frac{2\pi^2 k_B T}{\hbar\omega_c}\right) \qquad (S7)$$

k_B is the Boltzmann constant, $\hbar$ is the reduced Planck constant, ω_c is the cyclotron frequency defined by eB/m^*. The fitting of the temperature dependence of FFT peak intensity by eq. (S7) in the main manuscript is shown in Fig. S6, and Fig. S7 shows the V_g and n dependence of m^*. The error bars are obtained by the standard deviation of the fitting by eq. (S7) in the main manuscript. Note that in this study, the estimated cyclotron mass can be identified by the effective mass obtained from the energy dispersion because the s-orbitals of the transport carriers are isotropic. m^* in our InAs QW/(Ga,Fe)Sb is relatively heavier than that in a NM InAs QW in the same range of n, which is shown as a blue dashed line in Fig. S7[5]. This is possibly due to the s-d hybridization between the s-orbitals of the electron carriers in InAs and the d-orbitals of the localized Fe spins in (Ga,Fe)Sb[3]. Moreover, m^* does not show monotonic increase with n but rather stays constant. This is different from the general case of NM InAs QW, where m^* increases as n increases because of the non-parabolicity of the conduction band at the large n limit[4]. The reason for this non-monotonic n-dependence can be understood as follows: Although a negative V_g leads to decrease of the electron density n, it also enhances the overlapping of the electron wavefunction of the InAs QW with the local Fe spins at the InAs/(Ga,Fe)Sb interface[1]. This enlarged overlapping causes stronger s-d hybridization between the electron carriers of InAs (s-orbitals) and the local spins from (Ga,Fe)Sb (d-orbitals), which in turn increases m^*. This means that m^* decreases as n increases due to the s-d hybridization at the interface. Therefore, the m^* versus n relationship contains both effects of the non-parabolicity of the InAs conduction band and the s-d hybridization at the interface.

We present the phenomenological model for Fig. S7 based on the previous analytical approach of n-dependent m^* in the NM InAs QW[5] as:

$$\frac{m^*(n)}{m_0} = \frac{m^*(0)}{m_0}\sqrt{1 + \frac{4E_0^{EMA}}{E_g} + \frac{4\pi\hbar^2 n}{E_g m^*(0)}} + (C_0 - C_1 n^2), \tag{S8}$$

where $m^*(0)$ (= $0.026m_0$, m_0 is free electron mass) is an effective mass of the conduction band electrons at the Γ point[6], E_g is the band gap of InAs (= 0.42 eV)[6], E_0^{EMA} (= 58 meV for a 15 nm-thick InAs QW) is the subband energy quantized in the growth direction obtained by the effective mass approximation[5]. C_0 and C_1 (> 0) are fitting parameters. The first term represents the non-parabolicity of the conduction band dispersion in InAs, which is an increasing function of n. On the other hand, the second term represents the effect of *s-d* hybridization on n, which is approximated by a quadratic function of n. This is because the penetration P of the electron wavefunction of the InAs QW into the ferromagnetic (Ga,Fe)Sb side, which is estimated by our self-consistent calculation (See Fig. S8. and ref [1]), almost quadratically depends on n. Because the interfacial *s-d* hybridization occurs due to the penetration P, it is natural to assume that $P \propto m^*$ as a first order approximation. The fitting result is shown in Fig. S7, and C_0 and C_1 are 0.031 and 1.1×10^{-35} [cm^4]. From this model, we can obtain the n dependent m^* data, which will be a useful tool to design InAs/(Ga,Fe)Sb heterostructures for novel spintronics devices[1].

References

1. Takiguchi, K. *et al.* Giant gate-controlled proximity magnetoresistance in semiconductor-based ferromagnetic–non-magnetic bilayers. *Nat. Phys.* **15**, 1134 (2019).

2. Khosla, R. P. & Fischer, J. R. Magnetoresistance in degenerate CdS: Localized magnetic moments. *Phys. Rev. B* **2**, 4084 (1970).

3. Johnson, P. D. *et al.* Hybridization and the effective mass of quantum-well states in magnetic multilayers. *Phys. Rev. B* **50**, 8954 (1994).

4. Shoenberg, D. *Magnetic Oscillations in Metals*. (Cambridge University Press, 1984). doi:10.1017/CBO9780511897870.

5. Gauer, C. *et al.* Energy-dependant cyclotron mass in InAs/AlSb quantum wells. *Semicond. Sci. Technol.* **9**, 1580 (1994).

6. Madelung, O. *Semiconductors; Data Handbook*. (Springer). doi:10.1007/978-3-642-18865-7.

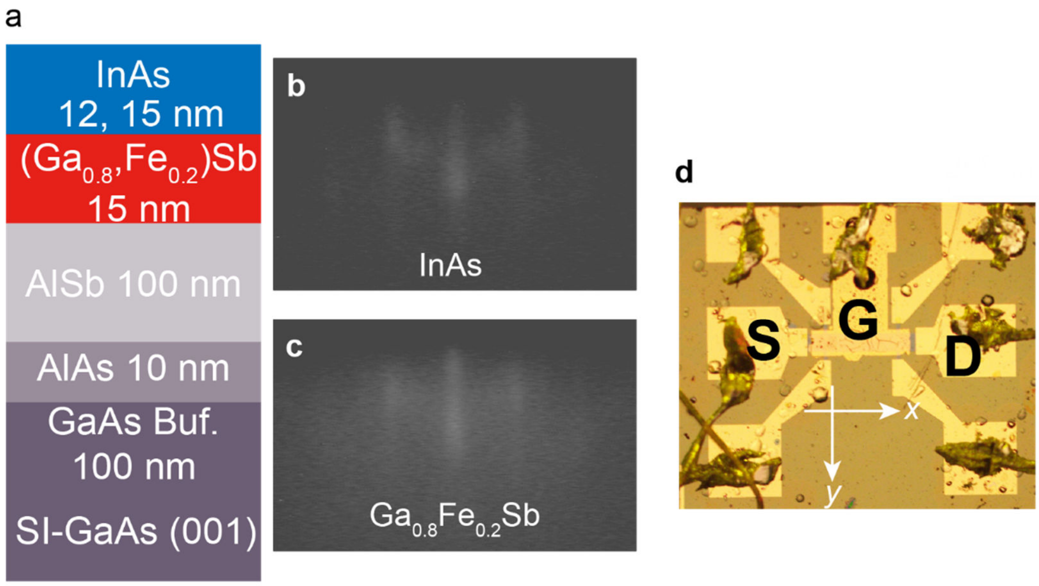

Figure S1 **a**, Schematic structure of sample A and sample B grown by molecular beam epitaxy (MBE) used in this study. **b**, RHEED patterns of InAs and **c**, that of (Ga,Fe)Sb in sample A. **d**, Optical microscopy image of sample A examined in this study. We apply an electrical current from the source (S) to the drain (D) and a gate voltage V_g between the gate electrode (G) and S.

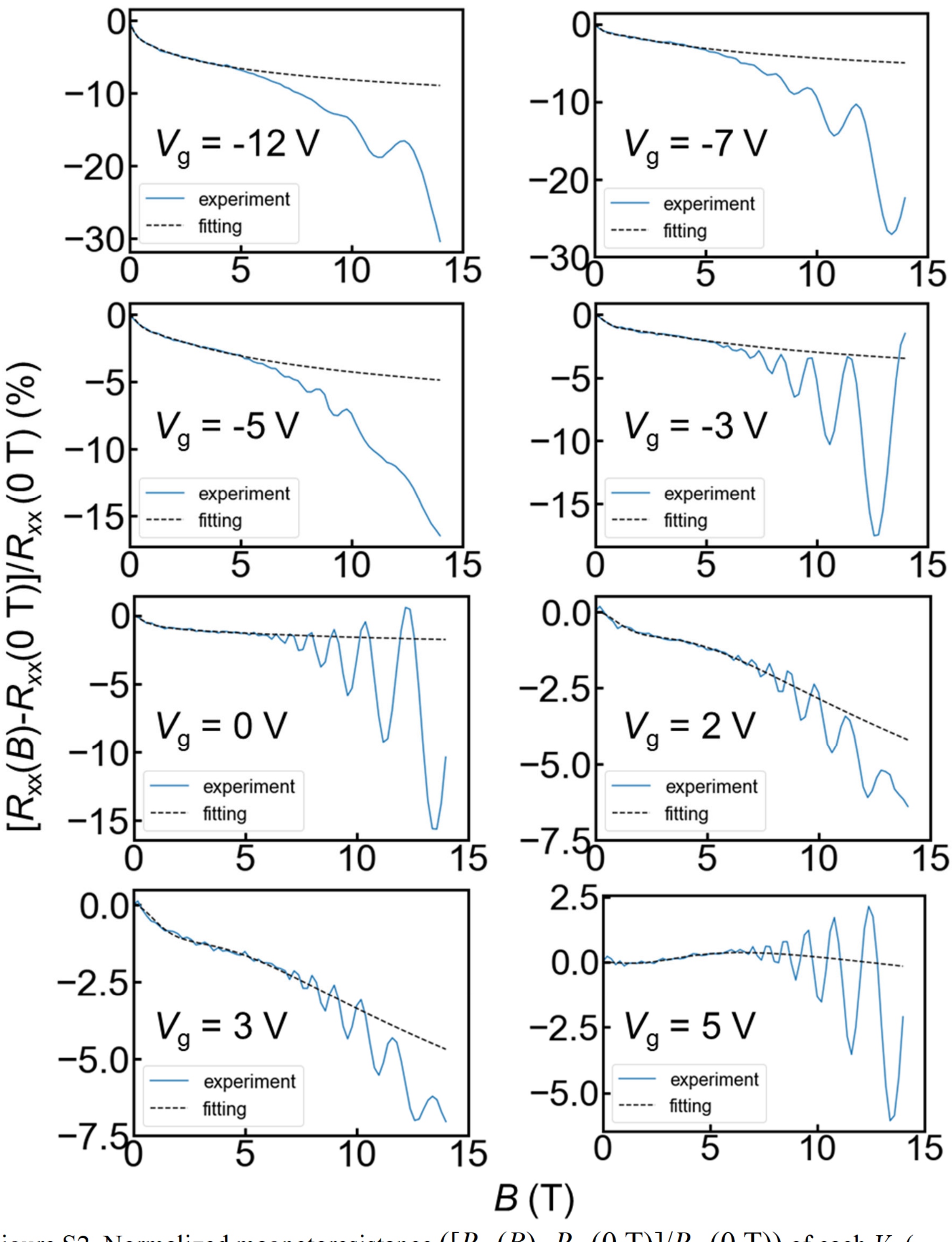

Figure S2 Normalized magnetoresistance ($[R_{xx}(B)-R_{xx}(0\text{ T})]/R_{xx}(0\text{ T})$) of each V_g (−12 ~ 5 V, blue curve) measured at 2 K and modified Khosla-Fisher fitting presented in eq. (S1) (black dashed line).

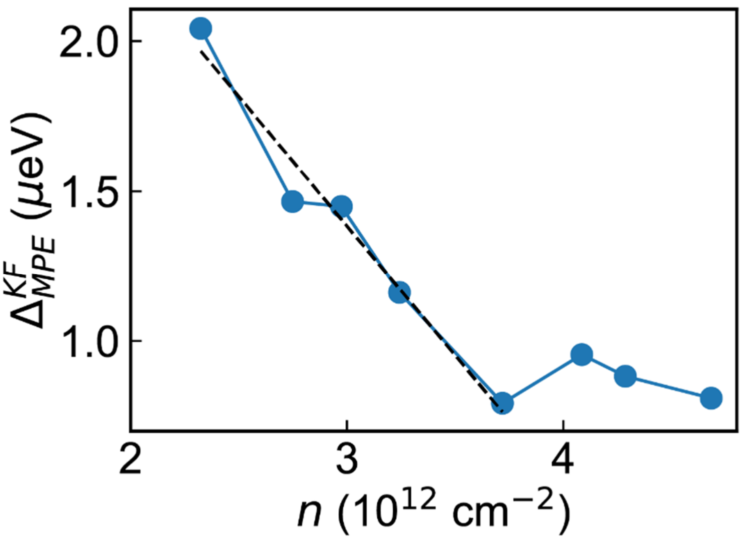

Figure S3 Carrier density n dependence of the spin splitting energy induced by MPE, $\Delta^{KF}{}_{\mathrm{MPE}}$, at 2 K estimated by the fitting from Fig. S6. In a lower n region, due to the negative V_g, the large penetration of the electron wavefunction of the InAs QW into the ferromagnetic (Ga,Fe)Sb layer is induced, leading to the increase in the spin splitting energy. The dashed line indicates that the $\Delta^{KF}{}_{\mathrm{MPE}} - n$ trend is linear in the lower n region where V_g is negative.

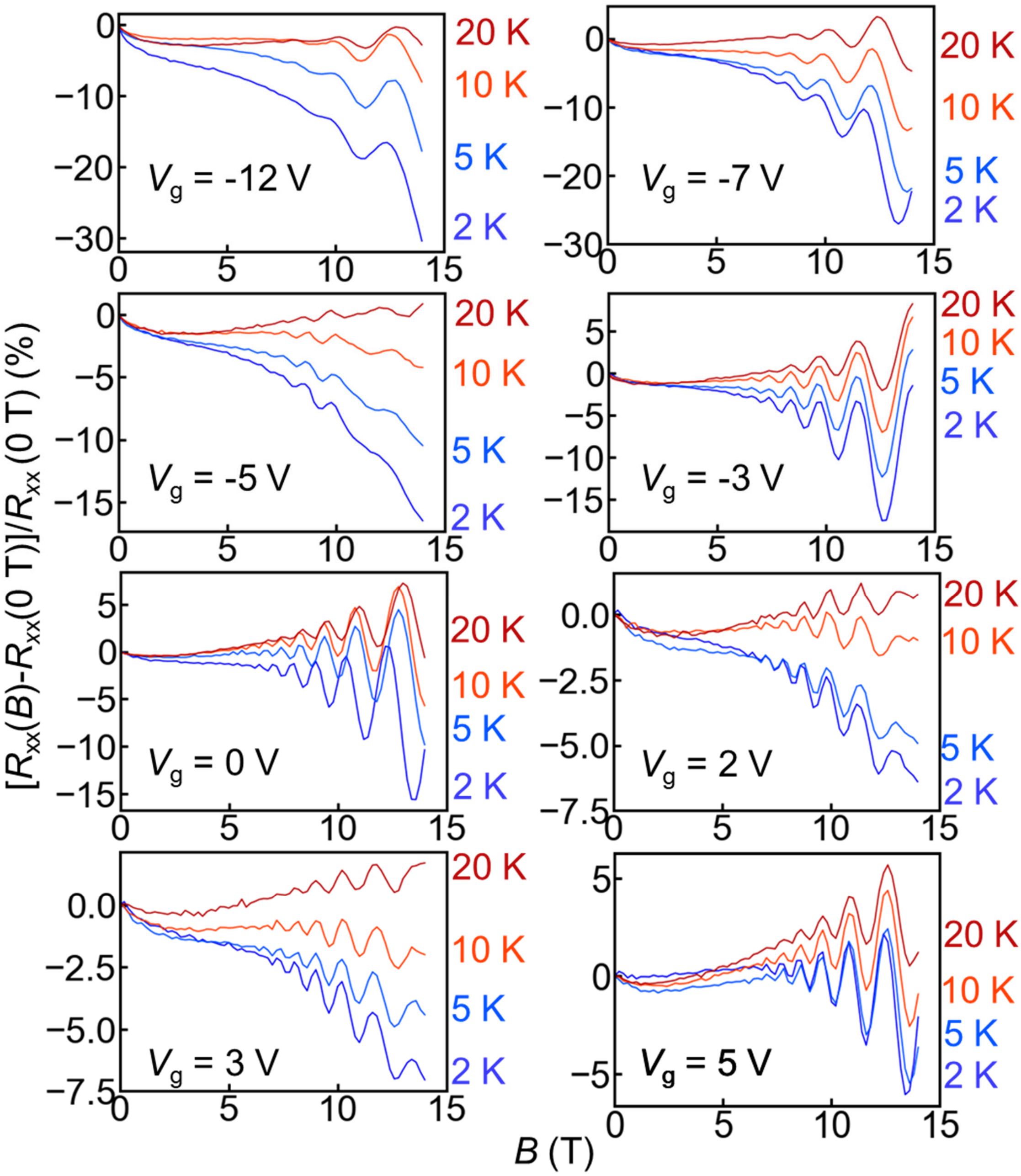

Figure S4 Normalized magnetoresistance (=$[R_{xx}(B) - R_{xx}(0\ \mathrm{T})]/ R_{xx}(0\ \mathrm{T})$) at various V_g (–12 ~ 5 V) and at various temperatures (T = 2 – 20 K).

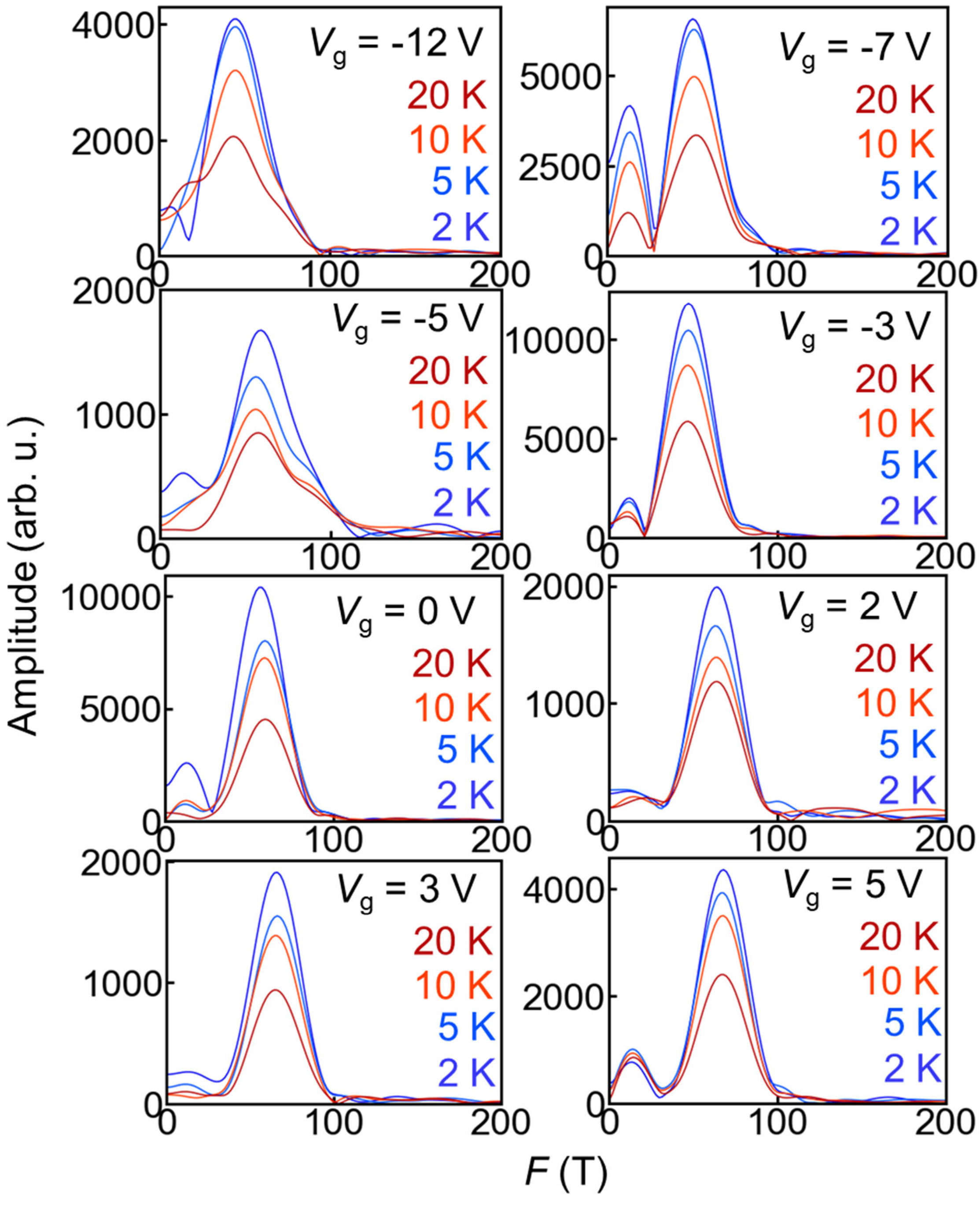

Figure S5 FFT spectra obtained from the oscillation components of Fig. S4 plotted against $1/B$ for each V_g at various temperatures (T = 2, 5 , 10, and 20 K). The longitudinal axis is the normalized amplitude of the FFT spectra, and the horizontal axis is the FFT frequency. The sub-peaks near F = 0 T may come from the background subtraction by polynomial fitting, thus they are not related with physical parameters.

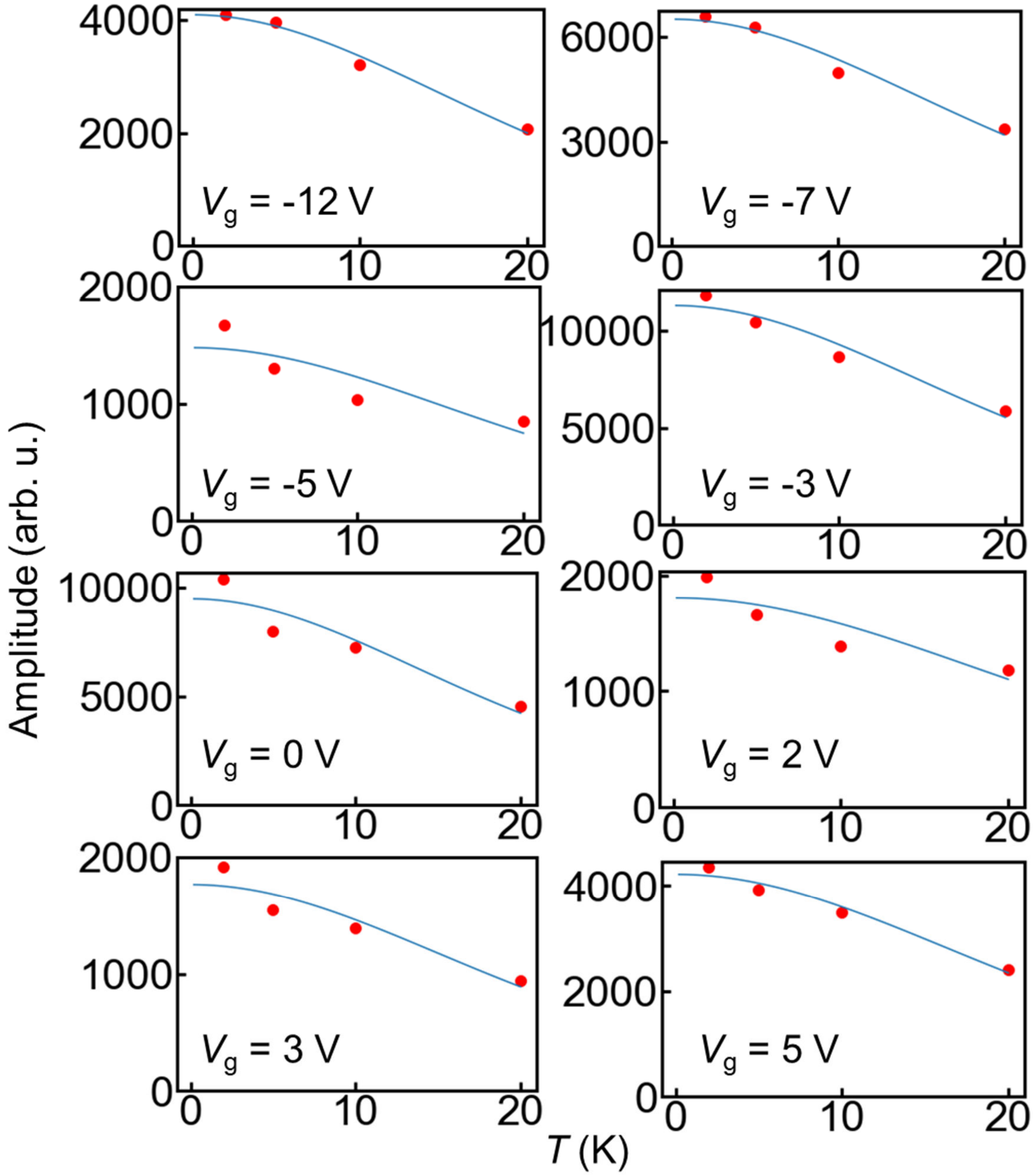

Figure S6 Temperature ($T = 2, 5, 10, 20$ K) dependence of the FFT peaks at each V_g. The blue lines represent the fitting curves obtained by eq. (S7).

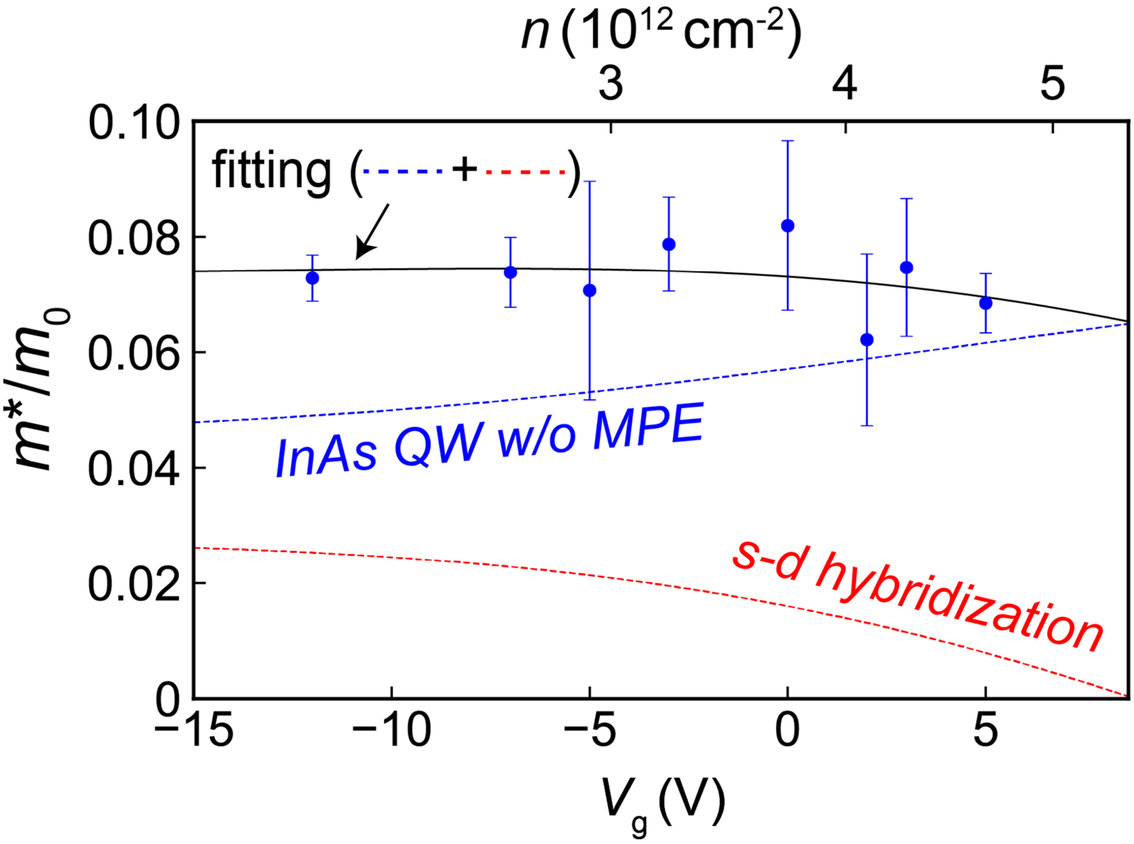

Figure S7 V_g and n dependence of the cyclotron mass m^*/m_0. The relation between V_g and n is shown in Fig. 3a. Each error bar is estimated from the standard deviation of the fitting of the temperature dependence of the SdH oscillations by eq. (S7). The black solid line indicates the fitting result of eq. (S8). The blue and red dashed lines indicate the first and second terms of eq. (S8) given by the fitting. The first term represents the effect of non-parabolicity in the energy dispersion of the InAs QW without MPE, and second term does the effect of MPE caused by the s-d hybridization.

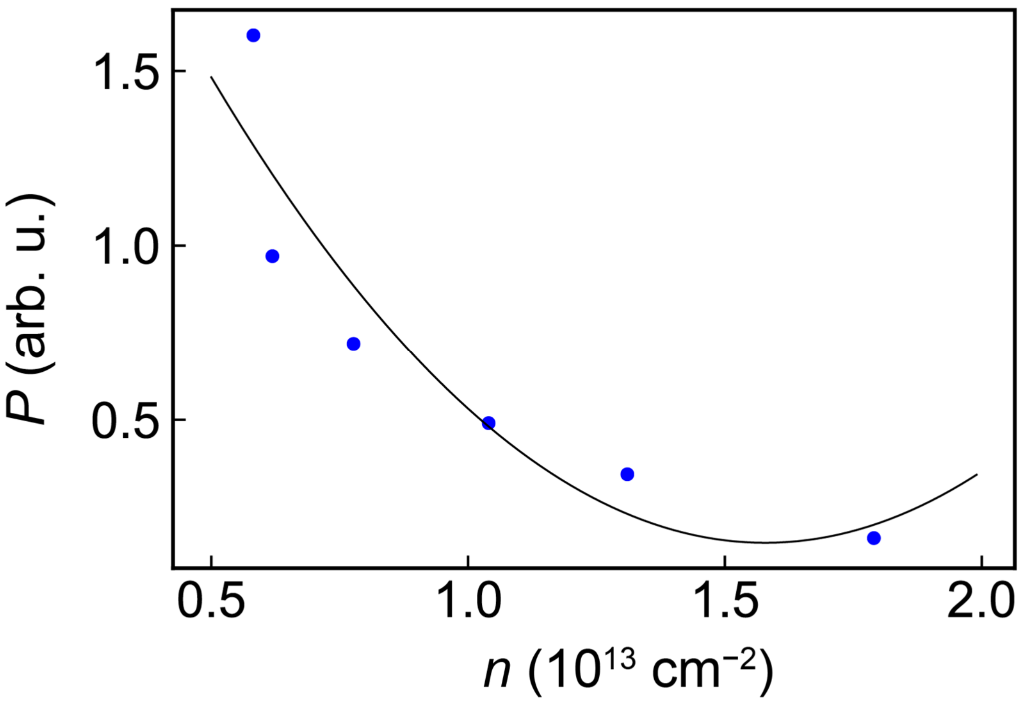

Figure S8 Penetration integral P of the electron wavefunction of the InAs QW into the ferromagnetic (Ga,Fe)Sb layer versus electron carrier density n, estimated from Ref. S1. The black solid line indicates the second polynomial fitting.